Unstructured Grid Simulations of Supersonic Mixing Using Ramp Injectors

Yoshiyuki KITAZUME[1] and Koji MIYAJI[2]
[1]Graduate school of Yokohama National University
[2]Lecturer, Yokohama National University
79-5 Tokiwadai, Hodogaya-ku, Yokohama, 240-8501, JAPAN
E-mail: k-dume@yal.asl.seg.ynu.ac.jp

Keywords:Supersonic Mixing, CFD, Grid Resolution

Abstract

This paper reports the grid resolution issues on the supersonic mixing simulation inside the engine for future aerospace vehicles. Unstructured finite volume method is used for the simulations. Three types of grids are used, namely, hybrid unstructured grids composed of prism and tetrahedron cells, locally refined grids, and hexahedral grids. Hexahedral grids are used to take advantage of fine distribution naturally behind the edge of the ramp where the vortex is generated. These latter two grids show much improved evaluations of the vortex motion and the mixing of the injected and the main flows.

1. Introduction

Innovative propulsion systems are required for future aerospace vehicles such as SSTO or TSTO. Supersonic combustion ram (SCRAM) jet engine[1,2] and rocket based combined cycle (RBCC) engine[3] are suggested as candidates for the vehicles. The key technology for the success of the both types of engines is the mixing of fuels and oxidizer (air) at supersonic speeds inside the engine. Numerical simulations have the advantage of changing the configuration of the engine or changing the physical conditions of the injection flow. However the simulation of supersonic mixing is difficult even for the state-of-the-art simulation technique and the validity of the simulation should be carefully examined for basic problems. The supersonic mixing of the injected and main flows modeling the internal flow of the engines is simulated using unstructured CFD method. The results are compared with the experiment[4,5] which was conducted at the propulsive engineering laboratory of Tohoku University. Figure1 shows the test section for the experiment. The ramp injector, which is shown in Fig. 2, is located inside the test section. The ramp angle against the lower wall is 30 degrees. The device is expected to enhance the mixing due to the longitudinal vortices generated at the edge of the ramp. In this simulation, both the main flow and the injection flow are used as air. Different types of the grid and the resolution issues are focused on for the accurate evaluation of the vortex decay and the mixing.

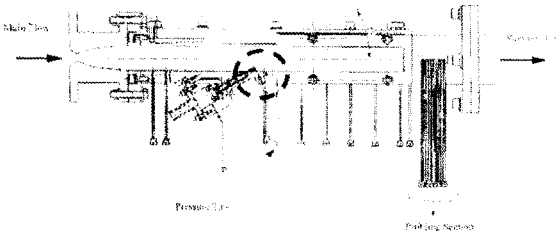

Fig. 1 test section

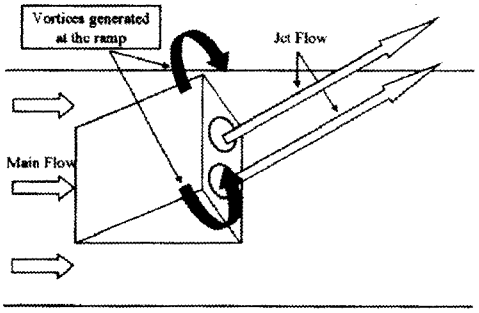

Fig. 2 Schematic of the ramp injector

2. Test section details and computational grids

The test section of the wind tunnel shown in Fig.1 starts at the nozzle exit and the shape of the section is a rectangular duct with 330[mm] length, and 30[mm] width and height. This ramp angle is 30 degrees against the lower wall. The length of the main flow direction (X-axis) and the width (Y-axis) are both 12[mm], the height (Z-axis) is 5.2[mm]. The diameters of the two-jet orifices are both 3.5[mm]. The length from the entrance of the test section to the injector's back-end is 225[mm], the length from this position to the exit of the test section is 105[mm].

Three types of the grids are used. First type is hybrid unstructured grids composed of prism and tetrahedron cells. Second type is the locally refined grid of the first type's grids. Last type is multi-block structured grids and covered to a single-block unstructured grids. These grids are respectively called "hybrid grids", "refined grids", and "hexahedral grids" in this paper. The "hexahedral grids" is used to take advantage of naturally fine distributions behind the edge of the ramp where the vortex is generated. An unstructured-grid approach for a structured-like grid has an advantage that it does not deteriorate the accuracy at the block interfaces.

The information of the grids is showen in Table 1.

Table 1 Number of grid points and cells

	Hybrid	Refined	Hexahedral
Grid Points	529380	2780654	1242972
Total Cell	1376468	13755032	1210233

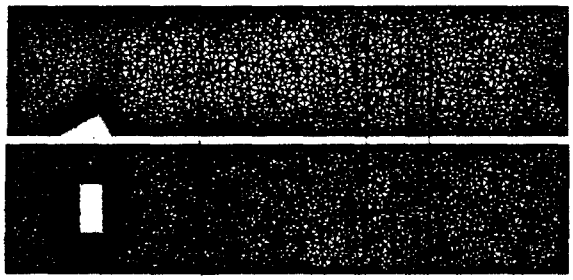

(a) Hybrid grids

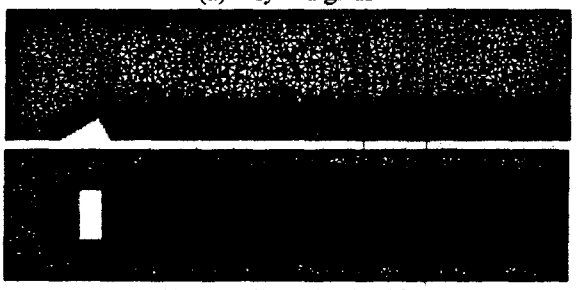

(b) Locally refined grids

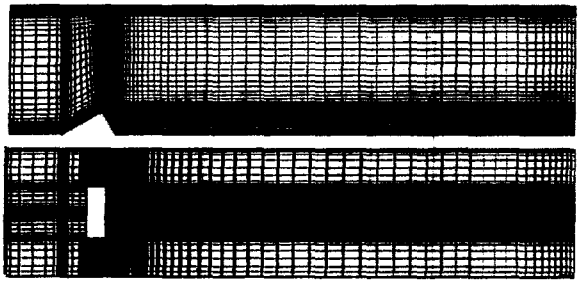

(c) Hexahedral grids

Fig. 3 the Y-section and Z-section crossed the ramp orifice's center

3. Numerical Algorithms

Three-dimensional Navier-Stokes equations for ideal gases are used as governing equations for the numerical simulations. The equation of the mass conservation for jet flow is simultaneously solved. The k-ω turbulence model[7] is used. The governing equations are expressed as follows.

$$\frac{\partial}{\partial t}\int_{\Omega} Q dV + \oint_{\partial\Omega}(F - F_v)dS = \int_{\Omega} s dV$$

$$Q = \begin{bmatrix} \rho \\ \rho u \\ \rho v \\ \rho w \\ e \\ \rho_j \\ \rho k \\ \rho\omega \end{bmatrix}, \quad F = \begin{bmatrix} \rho U \\ \rho u U + (p + \frac{2}{3}\rho k)n_x \\ \rho v U + (p + \frac{2}{3}\rho k)n_y \\ \rho w U + (p + \frac{2}{3}\rho k)n_z \\ (e + p + \frac{2}{3}\rho k)U \\ \rho_j U \\ \rho k U \\ \rho\omega U \end{bmatrix}$$

$$F_v = \begin{bmatrix} 0 \\ \hat{\tau}_{xx} \\ \hat{\tau}_{xy} \\ \hat{\tau}_{xz} \\ b_x \\ \rho D Y_{j,x} \\ \mu_k k_{,x} \\ \mu_\omega \omega_{,x} \end{bmatrix} n_x + \begin{bmatrix} 0 \\ \hat{\tau}_{yx} \\ \hat{\tau}_{yy} \\ \hat{\tau}_{yz} \\ b_y \\ \rho D Y_{j,y} \\ \mu_k k_{,y} \\ \mu_\omega \omega_{,y} \end{bmatrix} n_y + \begin{bmatrix} 0 \\ \hat{\tau}_{zx} \\ \hat{\tau}_{zy} \\ \hat{\tau}_{zz} \\ b_z \\ \rho D Y_{j,z} \\ \mu_k k_{,z} \\ \mu_\omega \omega_{,z} \end{bmatrix} n_z, \quad s = \begin{bmatrix} 0 \\ 0 \\ 0 \\ 0 \\ 0 \\ 0 \\ P_k - \beta_k \rho\omega k \\ P_\omega - \beta_\omega \rho\omega^2 \end{bmatrix}$$

$$e = \frac{p}{\gamma - 1} + \frac{\rho}{2}\left(u^2 + v^2 + w^2\right) + \rho k, \quad U = V \cdot n = u n_x + v n_y + w n_z, \quad Y_j = \frac{\rho_j}{\rho}$$

Cell-vertex finite-volume formulation is used for the spatial discretizations. Numerical fluxes for the invicid terms are the SHUS scheme and spatially 2nd order accuracy is attained by piecewise linear reconstructions of the primitive variables. The Venkatakrishnan's limiter is used. As a time integration method, Matrix-Free Symmetric Gauss-Seidel is used.

4. Flow conditions

Mach number of the main flow is set to 2.35 and Mach number of the injected flow is set to 2.0, as in the experiment. The dynamic pressure ratio of the injected flow to the main flow is 1.7. Reynolds number is 3.323×10^5 based on the height of the rectangular duct.

5. Results

5-1. Validation of grid relativity

In this section, the results on the three types of grids are compared.

Density contour plots and Schlieren photograph obtained by the experiment

Figures 4 (a)-(c) show the density contour plots in the Y-constant section passing the center of the ramp orifice. Figure 4 (d) shows the Schlieren photograph obtained by the experiment. The separated shear layer from the apex of the ramp is not observed on the initial hybrid grids in Fig. 4 (a) but it is clear in the results using the refined grids and the hexahedral grids shown in Figs. 4 (b) and (c). As for the resolution of the reflected shock wave from the lower wall, the results on the refined grids in Fig. 4 (b) is better than that on the hexahedral grids in Fig. 4 (c). The grid lines are not aligned for the oblique shock waves for the hexahedral grids and that is why the shock wave are smeared downstream. On the other hand, undirectional tetrahedral grids in the hybrid grids and the refined grids are better for the resolution of the oblique shock waves. The hexahedral grids have another defect, that is, many grid points are

distributed at unimportant or smooth flow region. It can be judged from Figs. 4 (a)-(c) that the refined grid is desirable for both the separated shear layer and the shock waves. The resolution can be further improved by adaptively refining the grids for the shock waves. But from the viewpoints of the computational costs, the tetrahedral and prism cells are expensive compared with hexahedral grids with the same number of grid points.

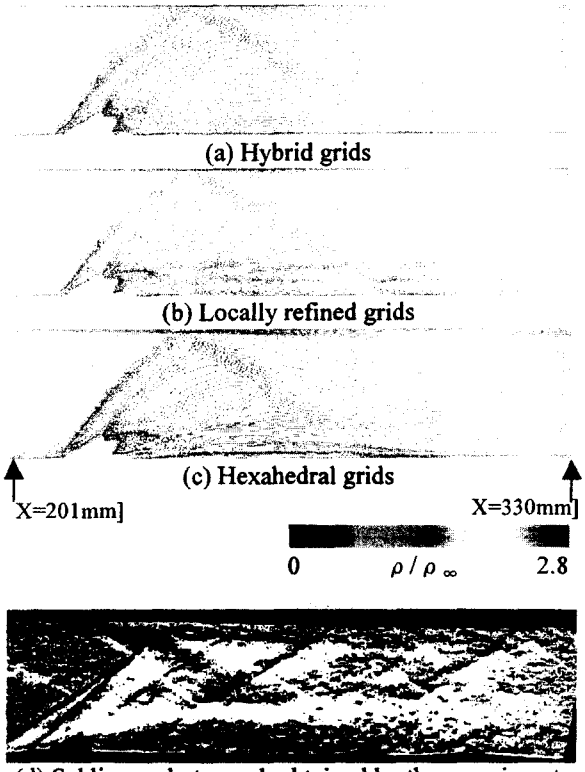

(d) Schlieren photograph obtained by the experiment

Fig. 4 density contour plots and Schlieren photograph (Y-section crossed by the ramp orifice's center)

Wall pressure distributions

Figure 5 shows the wall pressure distribution for the experiment and the simulations at the mid-span (Y-symmetry plane). The horizontal axis is the X-coordinate normalized by the diameter of the jet orifice. The vertical axis is the wall pressure normalized by the total pressure of the inlet air, namely, atmospheric pressure.

The sudden pressure increase at the foreface of the ramp is due to the shock wave ahead of the ramp. The rapid decrease just after the peak is due to the flow expansion at the apex of the ramp. Several recompressions are observed behind the ramp due to the reflected shock waves.

Only small numbers of points are available in the experiment and it is difficult to compare simulations with the experiment in detail. The quantitative discussion requires further checks of the accuracy for both the simulations and the experiment.

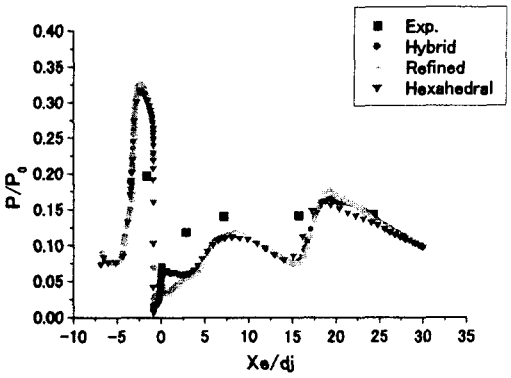

Fig. 5 wall pressure distribution (Y=0 line)

Velocity fields

Figures 6 (a)-(d) show the velocity vectors projected to streamwise-cross section (X-constant) at Xe/dj=4.3. The counter rotating vortices are well captured in all the simulations, which are generated at the apex of the ramp.

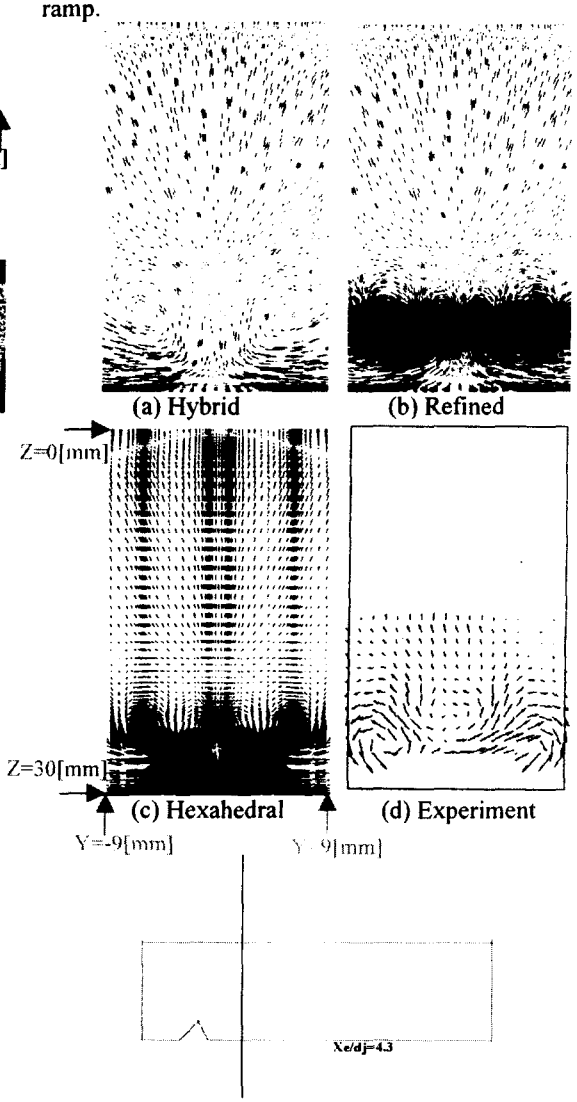

Fig. 6 Velocity vectors at Xe/dj=4.3

Figures 7 (a)-(d) shows the iso-surface of the velocity components in Y-direction (component v). The measurement area is in the framed red line of the bottom figure. The cyan region shows the iso-surface on which v=-50 and the yellow region shows the iso-surface on which v=50. In Fig. 7 (d) showing the experimental result, the yellow surface exists over the cyan surface at the left side of the symmetry plane (positive Y), on the contrary, the cyan area exists over the yellow area at the right side of the symmetry plane (negative Y). It means the flow run apart near the lower wall and the flow run ahead at the upper region in the regions considered in Figs. 7. They are again due to the pair of vortices generated at the apex of the ramp.

In the result on hybrid grids, the characters are not captured. While in the results on the refined grids and the hexahedral grids, they are correctly simulated and it shows the significant importance of the grid resolution near the shear layers from the apex of the ramp.

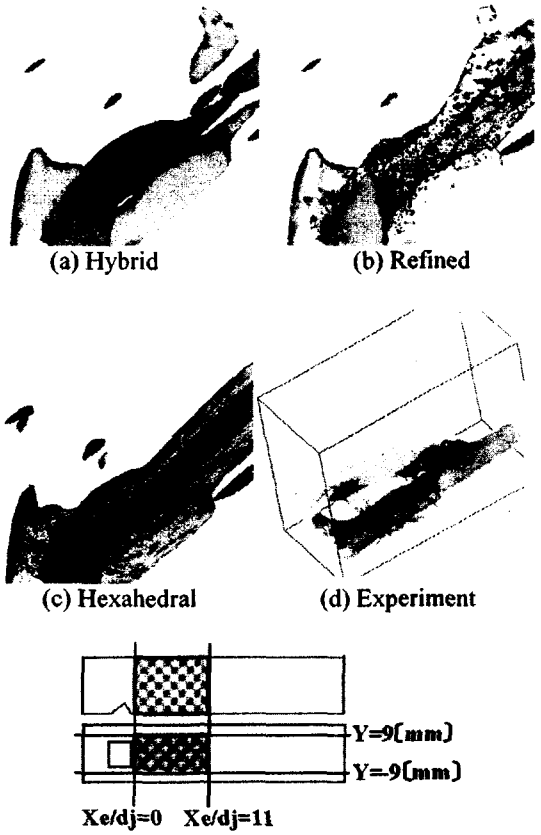

Fig. 7 velocity isosurface(v=-50,50[m/s])

Mass-fraction contour plots

Figures 8 and 9 are the mass-fraction of the computational results and the experiment at Xe/dj=15 and 30, respectively. In the experiment, the mass-fraction is calculated by using the density distribution of helium that is obtained by gas chromatography's method although all the above results use air as the injected gas. And so, quantitative comparison is impossible for Figs. 8 and 9 but qualitative comparisons are shown.

At Xe/dj=15 (Fig.8), twin injected flows are independent and the mixing has not occurred so far in Figs. 8 (b), (c) and (d). The contour lines by the hybrid grids is laterally extended and they qualitatively differ from others.

At Xe/dj=30 (Fig.9), the merging of the twin injected flow proceeds and the resulting contours do not show independent cores in the experiment in Fig. 9 (d). At this section, the result by the hybrid grids happens to be similar to the experiment, but it is thought from the comparison of Fig. 8 (a) and Fig. 9 (a) that excessively diffused vortices are just conveyed downstream. In Figs. 9 (b) and (c), the vortex merging proceeds but independent cores still exist. It is due to the difference of the injected gas flow from the experiment. The higher density in the simulation results in the less vortex merging, although the dynamic pressure ratio of the main flow to the injected flow are the same as the experiment. In addition, the flow asymmetry is observed in Fig. 9 (c), and it requires further investigation on the grid resolutions.

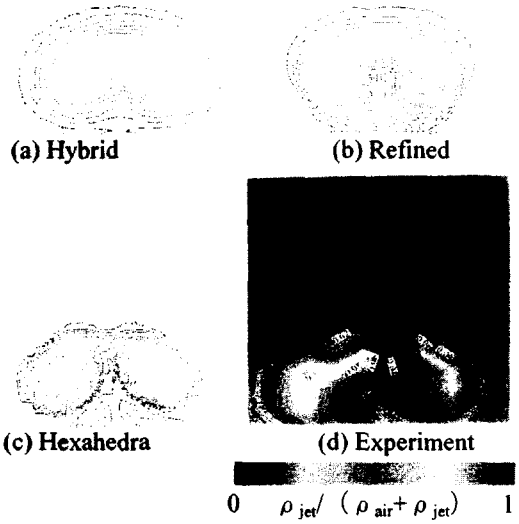

Fig. 8 mass-fraction (Xe/dj=15)

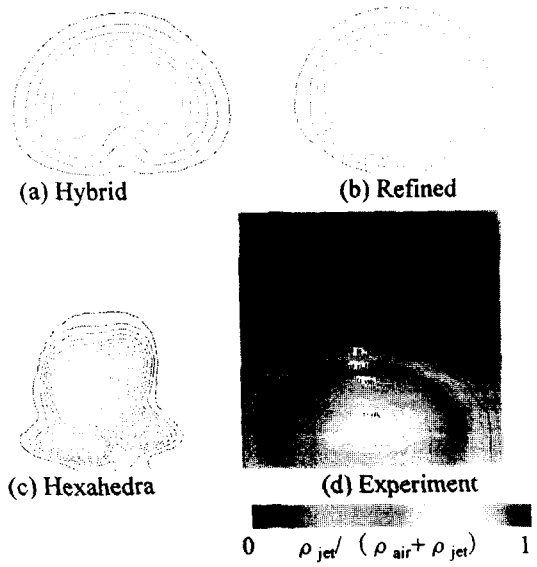

Fig. 9 mass-fraction (Xe/dj=30)

5-2. Vortex motion and the mixing of the main flow and the injected flow

It is concluded from the above discussion that the locally refined grids for the hybrid grids is the best among the three simulations. In this section, the relation between the longitudinal vortex and the mixing of the main flow and the injected flow is examined with the results on the refined grids. The mass-fraction at the Y=0 cross section and the Z-constant cross section passing the center of the orifice are shown in Figs. 10 (a) and (b).

The contour lines near the lower wall in Fig. 10 (a) section is first deflected upward and then pressed to downward. The upper boundary is also deflected upward and downward. They are due to both the rolling up of the vortex and the shock wave impingement to the jet flow. In Z-constant section, the symmetrically separated high mass-fraction regions are observed downstream corresponding to the deflected contours in Fig. 10 (a). In addition the high mass-fraction regions begin to merge near the exit plane in Fig. 10 (b).

The relations between the vortex motion and the mixing are examined by investigating the flows in X-constant cross sections. Figures 11, 12 and 13 show the mass-fraction, the total-pressure and the velocity vector's, respectively. The growth of the vortices is seen in Figs.12 and 13. The vortex shape is similar to the mass-fraction distributions, which directly show the degree of the mixing. So, the vortex motion is closely related to the mixing of main flow and injected flow. The figures show the longitudinal vortex motion efficiently enhances the mixing. When the vortex is decayed and diffused, the mass fraction approaches homogeneous and the mixing is enhanced more.

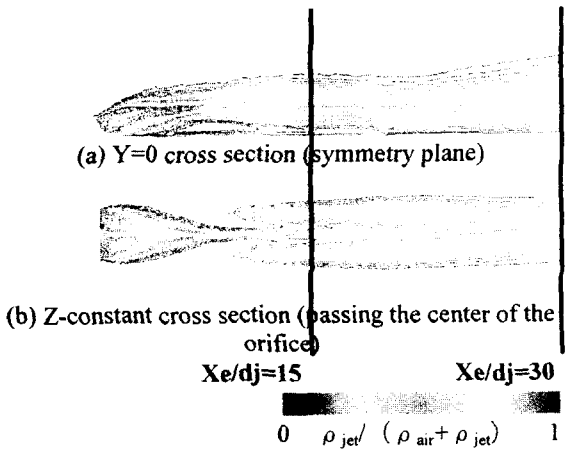

Fig. 10 mass-fraction of Y-section and Z-section

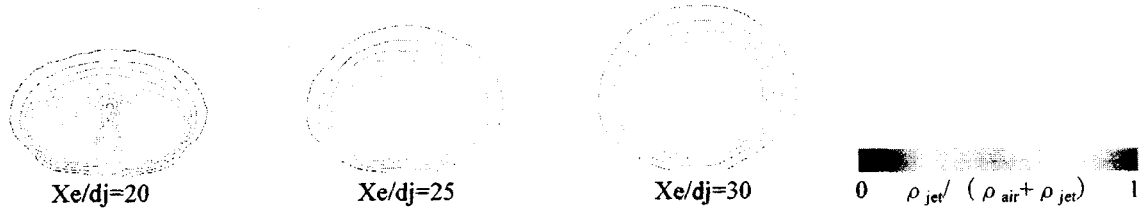

Fig. 11 mass-fraction of X-section

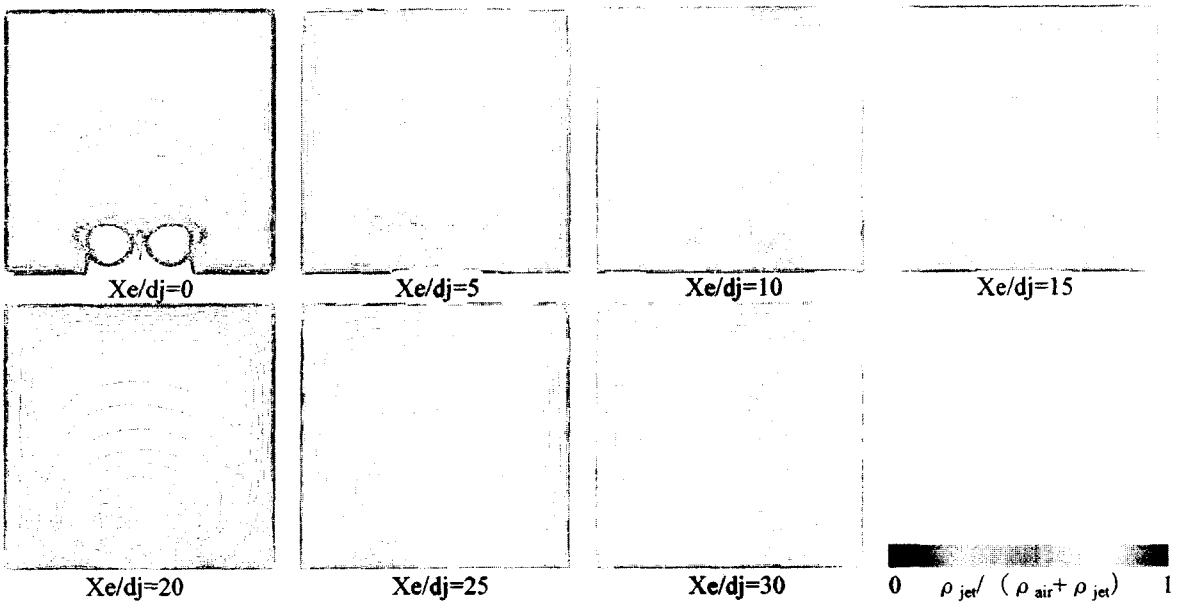

Fig. 12 total-pressure contour plots of X-section

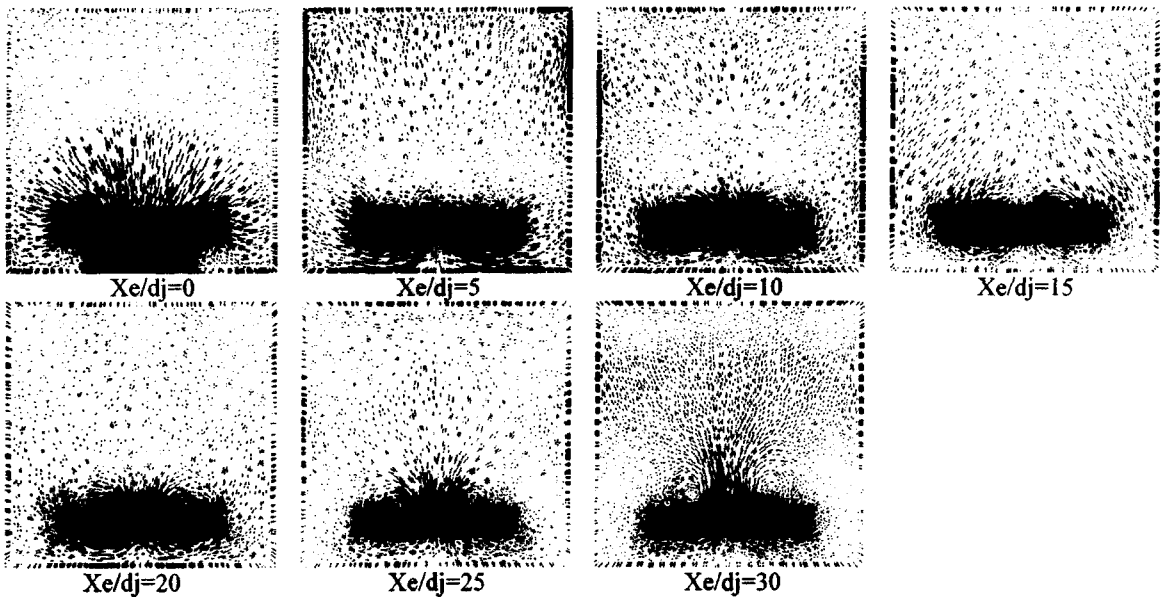

Fig. 13 velocity vector projected X-sectio

6. Summary

In this paper, the computations of the supersonic mixing using longitudinal vortices are carried out to simulate the internal flow of the future aerospace engine. With the aim of the accurate simulation of the mixing of the main flow and the injected flow, the grid resolution issues are mainly discussed. The conclusions of the paper are summarized as follows.

- Both the refined grids and the hexahedral grids simulate the separated shear layers behind the ramp, but the resolution is not satisfactory for the second reflected shock waves in hexahedral grid. Moreover, many grid points are used at unimportant or smooth flow region for the latter grid.
- In the refined grids, the grid points are efficiently distributed and the resolution of both the separated shear layer and the shockwaves are well captured. The computational cost for the grid is, however, high compared with the hexahedral grids with the same number of grid points.
- It has been shown that a pair of vortices generated at the edge of the ramp efficiently mixes the two flows. The mixing is enhanced as the vortices diffuse downstream.

References

1) Heiser, H. W., and Pratt, D. T., "Hypersonic Airbreathing Propulsion," AIAA Education Series.
2) Kodera, M., Sunami, T., and Scheel, F., "Numerical Study on The Supersonic Mixing Enhancement Using Streamwise Vortices," 16th Numerical fluid dynamics symposium collected paper,2002. (in Japanese)
3) Yamanaka, T., Maita, M., Mori, T., Tsuchiya, T., and Okamoto, O., "An ARCC Engine Powered Spaceplane," AIAA Paper 2001-1923,2001.
4) Suzuki, K., "Study of Velocity Field Produced by Twin Jets Injected from a Ramp Injector in a Supersonic Flow," Master Dissertation, Dept. of Aerospace Engineering, Tohoku university, 2003. (in Japanese)
5) Yaguchi, H., "Mixing of Swirling Jet Flow Injected from a Ramp Injector," Master Dissertation, Dept. of Aerospace Engineering, Tohoku university, 2000. (in Japanese)
6) Miyaji, K., "Prediction of Hypersonic Shock/Shock Interaction Heating Using Hybrid Adaptive Unstructured Grids," 10th AIAA International Space Planes and Hypersonic Systems and Technologies Conference, AIAA Paper 2001-1751,2001.
7) Wilcox, D.C., "Reassessment of Scale-Determining Education for Advanced Turbulence Models," AIAA J., 26(1988), pp.1299-1310.
8) Kitazume, Y., and Miyaji, K., "Grid Resolution Issues on the Supersonic Mixing Simulation," 17th Numerical fluid dynamics symposium collected paper, 2003. (in Japanese)